




Preparation of a novel composite g-C₃N₄/TiO₂/NiWO₄ with enhanced photocatalytic activity toward the degradation of rhodamine B

Hao-chen Gu¹, Yu-bin Tang^{1,*}, Fang-yan Chen^{1,*} , Ming-yang Li¹, and Wei-long Shi²

¹ School of Environmental and Chemical Engineering, Jiangsu University of Science and Technology, Zhenjiang 212100, Jiangsu, People's Republic of China

² School of Materials Science and Engineering, Jiangsu University of Science and Technology, Zhenjiang 212100, Jiangsu, People's Republic of China

Received: 11 February 2022

Accepted: 5 May 2022

Published online:
25 May 2022

© The Author(s), under exclusive licence to Springer Science+Business Media, LLC, part of Springer Nature 2022

ABSTRACT

A novel ternary heterojunction composite photocatalyst g-C₃N₄/TiO₂/NiWO₄ was fabricated using a simple hydrothermal method. The synthesized samples were characterized using X-ray diffraction (XRD), scanning electronic microscopy (SEM), energy-dispersive spectrum (EDS), Fourier transform infrared spectroscopy (FT-IR), X-ray photoelectron spectroscopy (XPS), ultraviolet–visible (UV–Vis) absorption spectra, photoluminescence (PL) spectra, transient photocurrent responses, and electrochemical impedance spectroscopies (EIS). The results indicated that the composite of g-C₃N₄/TiO₂/NiWO₄ had been successfully synthesized. By constructing a ternary heterojunction, the electron migration rate and light absorption of the material are further improved; the photogenerated electron–hole recombination is inhibited. The ternary composite photocatalyst shows the highest photocatalytic activity for the degradation of rhodamine B (RhB) than that of g-C₃N₄, TiO₂, NiWO₄, and g-C₃N₄/TiO₂ photocatalyst. The degradation efficiency of RhB using g-C₃N₄/TiO₂/NiWO₄ can reach 99% after visible-light irradiation for 40 min. Finally, the migration mechanism of charge carriers in the ternary system has been schematically illustrated by the active species capture experiment. Our research can pave the way for the fabrication of ternary heterojunction composite photocatalyst with high photocatalytic activity for the environmental contaminants treatment.

Address correspondence to E-mail: tangyubin@just.edu.cn; chenfangyan@just.edu.cn

1 Introduction

As a traditional photocatalyst, TiO_2 has been widely researched due to its high chemical and thermal stability, non-toxicity, higher activity, lower cost and environmentally friendly advantages [1–3]. However, the practical applications of TiO_2 was limited due to its some intrinsic disadvantages, such as lower quantum efficiency, relatively wide bandgap only being excited by ultraviolet light and rapid recombination of photogenerated electron–hole pairs on the surface or in the lattice of TiO_2 , etc., so many efforts have been made to improve its photocatalytic performance and photoelectric conversion efficiency [4, 5], including hydrogenation modified TiO_2 , energy band modulation by doping with some metal elements and non-metal elements [6], etc. Combining TiO_2 with other semiconductor which possesses narrow bandgap to fabricate heterojunction composite photocatalyst is considered to be a simple and effective method to improve the photocatalytic activity [7].

In recent years, the development of visible light-driven composite materials has become a hot spot in solar photocatalysis research field. $\text{g-C}_3\text{N}_4$ is a kind of non-metal polymerized semiconductor with a narrow bandgap (2.7 eV) which can be excited by visible light, and it has great application potential in the fields of photocatalytic hydrogen production, carbon dioxide conversion, and degradation of organic pollutants retained in the environment [8, 9]. Unfortunately, pure $\text{g-C}_3\text{N}_4$ exhibits poor photocatalytic performance due to lower separation efficiency of photogenerated electron–hole pairs. But fortunately, $\text{g-C}_3\text{N}_4$ has a suitable band position which matches well with that of TiO_2 .

Constructing heterojunction, doping and loading catalyst are modification strategy for $\text{g-C}_3\text{N}_4$ and TiO_2 [10, 11]. To construct $\text{TiO}_2/\text{g-C}_3\text{N}_4$ heterojunction not only can broaden the light response range of TiO_2 -based photocatalyst but also can effectively suppress recombination of photogenerated electron–hole pairs [12]. Up to now, there are many researches on the synthesis and modification of the composite $\text{g-C}_3\text{N}_4/\text{TiO}_2$. Zhang et al. loaded $\text{g-C}_3\text{N}_4$ onto a TiO_2 nanotube array by a simple electrodeposition method and exhibited excellent photocatalytic hydrogen evolution activity [13]. Wang et al. prepared $\text{g-C}_3\text{N}_4/\text{TiO}_2$ nanomaterials by using high-voltage electrospinning and hydrothermal methods. They treated the surface of pure nano- TiO_2 by acidification before

it was combined with $\text{g-C}_3\text{N}_4$. The results showed that the photocatalytic activity of the $\text{g-C}_3\text{N}_4/\text{TiO}_2$ nanocomposite treated by acidification is much higher than that of the untreated catalyst [14]. Tan et al. prepared nanostructured $\text{g-C}_3\text{N}_4/\text{TiO}_2$ through a one-step method, which can improve hydrogen production efficiency under visible light [15]. Zhang et al. prepared ternary $\text{MoS}_2/\text{g-C}_3\text{N}_4/\text{TiO}_2$ nanosheet composites by liquid stripping and solvothermal methods [16]. Compared with binary photocatalyst, the ternary composites have higher photogenerated carrier separation rates and faster electron migration rates [17]. Wu et al. synthesized heterojunction photocatalyst $\text{g-C}_3\text{N}_4/\text{TiO}_2/\text{HNTs}$ which can efficiently catalyze the degradation of ciprofloxacin in water [18]. However, the reports on ternary photocatalysts with high stability, low cost, and excellent catalytic performance are still scarce.

Recently, a series of low-cost metal tungstates such as Bi_2WO_6 , CuWO_4 , NiWO_4 , and CoWO_4 have been widely studied due to their excellent optical, electrical, magnetic, and catalytic properties [19–22]. Among them, NiWO_4 , as a simple and common tungstate material, possess the narrow bandgap and can make full use of the solar radiation energy, has been applied in many fields, including sensors, catalysts and supercapacitors [23]. Many researchers have used NiWO_4 as photocatalyst for the degradation of organic pollutants in the environments [20].

In the present paper, we designed and synthesized a novel ternary heterojunction composite photocatalyst $\text{g-C}_3\text{N}_4/\text{TiO}_2/\text{NiWO}_4$ by using a simple hydrothermal method for the degradation of rhodamine B (RhB) in aqueous solutions. The electron migration rate and light absorption of the material prepared are improved, and the photogenerated electron–hole recombination is inhibited, compared with that of the photocatalyst $\text{g-C}_3\text{N}_4$, TiO_2 , NiWO_4 , and $\text{g-C}_3\text{N}_4/\text{TiO}_2$. This work provides a new way for the preparation of ternary heterojunction composite photocatalyst with high photocatalytic activity and for the treatment of contaminants in the environment.

2 Experimental section

2.1 Materials employed

Melamine, absolute ethanol, tetra-*n*-butyl titanate, nickel nitrate ($\text{Ni}(\text{NO}_3)_2 \cdot 6\text{H}_2\text{O}$), sodium tungstate

($\text{Na}_2\text{WO}_4 \cdot 2\text{H}_2\text{O}$), and rhodamine B were all purchased from Sinopharm Group Chemical Reagent Co., Ltd. (Shanghai China). All the chemicals employed were of analytical grade.

2.2 Synthesis of the photocatalysts

The $\text{g-C}_3\text{N}_4$ was prepared by the thermal polycondensation method. In a typical synthesis, 1 g of melamine was heated at 500 °C for 120 min at the rate of 10 °C/min in a crucible with a cover, and then cooled to room temperature. The sample was then ground into the powder for further use.

The $\text{g-C}_3\text{N}_4/\text{TiO}_2$ was synthesized by the hydrothermal method. Firstly, 50 mg of the as-prepared $\text{g-C}_3\text{N}_4$ were dispersed into 70 mL of absolute ethanol; the mixture was then stirred by ultrasound for 5 min. Then, under the condition of continuous magnetic stirring, 1 mL of tetra-*n*-butyl titanate reagent was slowly added dropwise to the $\text{g-C}_3\text{N}_4$ /absolute ethanol mixture, and then continued to stir the mixture for 2 h. After that, the resulting mixture was transferred into a Teflon-lined stainless steel vessel with a capacity of 100 mL and heated at 200 °C in an oven for 20 h. Then the product was cooled to room temperature, the obtained solid samples were collected by centrifugation with distilled water and ethanol for several times. Finally, dried in a vacuum oven at 80 °C for 24 h, the resultant pale-yellow solid powder was $\text{g-C}_3\text{N}_4/\text{TiO}_2$ labeled as CT.

For synthesis of the ternary composite $\text{g-C}_3\text{N}_4/\text{TiO}_2/\text{NiWO}_4$, 0.13 g of $\text{Ni}(\text{NO}_3)_2 \cdot 6\text{H}_2\text{O}$ and 0.15 g of $\text{Na}_2\text{WO}_4 \cdot 2\text{H}_2\text{O}$ were separately dispersed in 30 mL deionized water, and remarked as solution A and solution B, respectively. Then, a known quantity of the prepared $\text{g-C}_3\text{N}_4/\text{TiO}_2$ solid powder was dispersed in the solution A, and stirred for 1 h. After that, solution B was slowly added dropwise to the above mixture, then heated to 80 °C and stirred for 2 h. The resulting mixture was transferred into a Teflon-lined stainless steel vessel with a capacity of 100 mL and heated at 200 °C for 20 h. The product was then cooled to room temperature; the obtained solid samples were collected by centrifugation with distilled water and ethanol for several times. Finally, dried in a vacuum oven at 60 °C for 24 h, the resultant green solid powder was $\text{g-C}_3\text{N}_4/\text{TiO}_2/\text{NiWO}_4$.

2.3 Characterization of catalysts

2.3.1 XRD

At room temperature, small angle diffraction was performed using an X'Pert-Pro MPD (Holland) D/max- γ A X-ray diffractometer with Cu $K\alpha$ radiation ($\lambda = 0.154178$ nm), and the scanning rate was 1°/min, with 2θ range of 10–70°.

2.3.2 FT-IR

The infrared spectra of the samples were determined by a Nicolet-360 Fourier transform infrared spectroscopy (FT-IR) by diffuse reflectance scanning technique from 4000 to 500 cm^{-1} .

2.3.3 SEM

The morphology and structure of the as-prepared samples were examined by Scanning electron microscopy (SEM, JSM-6360LV, JEOL Japan).

2.3.4 EDS

The energy-dispersive X-ray spectra (EDS) were carried out by the JSM-6360LV microscope.

2.3.5 PL spectra

Photoluminescence (PL) spectra of the as-prepared samples were recorded by a RF-5301PC luminescence spectrometer excited with 320 nm wavelength.

2.3.6 XPS

X-ray photoelectron spectroscopy (XPS) were acquired on an ARL Quant X-ray photoelectron spectrometer using Al $K\alpha$ X-ray ($h\nu = 1486.6$ eV).

2.3.7 UV-Vis

UV-Vis absorption spectra of the samples were recorded on a Lambda 750 (Perking Elmer) spectrophotometer in the tested range of 200–800 nm.

2.3.8 Electrochemical test

The electrochemical test was use a typical three-electrode system and carried out by a CHI 660b workstation.

2.3.9 Photocatalytic activity test

First, 50 mg of photocatalyst was placed into a 100 mL of RhB aqueous solutions (10 mg/L) and stirred for 30 min in a dark environment to achieve adsorption–desorption equilibrium. Then, a 300 W xenon lamp with a 420 nm cut filter was chosen as a visible-light source. At certain time intervals, 5 mL of aliquots were extracted and centrifuged, and then, analyzed by using UV–Vis spectrophotometer at a maximum absorption wavelength of 553 nm. The degradation efficiency (DE) of RhB was calculated using the formula: $DE (100\%) = (1 - c/c_0) \times 100\%$, where, c is the concentration of RhB at each irradiation time interval and c_0 is the initial concentration.

3 Result and discussion

3.1 Crystal structure and morphology

The XRD patterns of the as-prepared samples $g\text{-C}_3\text{N}_4$, $g\text{-C}_3\text{N}_4/\text{TiO}_2$ and $g\text{-C}_3\text{N}_4/\text{TiO}_2/\text{NiWO}_4$ are shown in Fig. 1.

It can be seen from Fig. 1 that $g\text{-C}_3\text{N}_4$ show two distinct characteristic peaks at 12.9° and 27.44° , corresponding to the (100) crystal plane of the hexazine heterocyclic unit and the (002) graphite layer stacked crystal plane, respectively, which is consistent with previous literature report [24]. $g\text{-C}_3\text{N}_4/\text{TiO}_2$ exhibit the overlapped characteristic peaks of both $g\text{-C}_3\text{N}_4$ and TiO_2 , indicating the successful synthesis of the binary composite [25]. As for $g\text{-C}_3\text{N}_4/\text{TiO}_2/\text{NiWO}_4$,

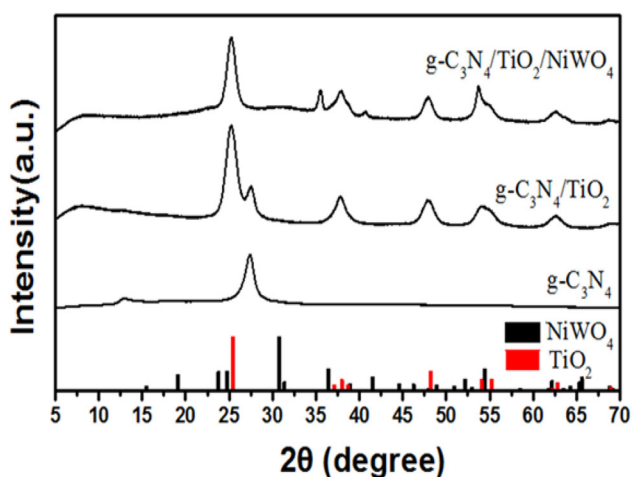


Fig. 1 XRD patterns of $g\text{-C}_3\text{N}_4$, $g\text{-C}_3\text{N}_4/\text{TiO}_2$ and $g\text{-C}_3\text{N}_4/\text{TiO}_2/\text{NiWO}_4$

the characteristic peak of $g\text{-C}_3\text{N}_4$ at 27.44° disappeared, and meanwhile, three new diffraction peak appeared at 35.4° , 40.7° , and 53.6° [26]; compared with the standard XRD card of NiWO_4 , the three new diffraction peaks correspond to the characteristic peaks of NiWO_4 at 36.5° , 41.8° , and 54.7° respectively, which demonstrated that the characteristic peak of $g\text{-C}_3\text{N}_4$ is covered after loading NiWO_4 . It also shows that a new ternary composite $g\text{-C}_3\text{N}_4/\text{TiO}_2/\text{NiWO}_4$ was successfully fabricated via compounding NiWO_4 and $g\text{-C}_3\text{N}_4/\text{TiO}_2$. All of characteristic peaks of NiWO_4 are shifted about 1.1° to the small angle of 2θ , while the positions of other characteristic peaks remain unchanged, indicating that the residual stress exist in the material during the material compounding process. Therefore, the crystal lattice of NiWO_4 is distorted, and the cell parameters and crystal surface spacing become larger. So that the characteristic peaks of NiWO_4 are collectively shift to the negative position.

The morphology of $g\text{-C}_3\text{N}_4$, $g\text{-C}_3\text{N}_4/\text{TiO}_2$, and $g\text{-C}_3\text{N}_4/\text{TiO}_2/\text{NiWO}_4$ was investigated by means of SEM technique, respectively. $g\text{-C}_3\text{N}_4$ shown in Fig. 2a presents an irregular stacked sheet-like structure with a diameter range from 100 nm to several micrometers. As can be seen from Fig. 2b and c, $g\text{-C}_3\text{N}_4/\text{TiO}_2$ shows the peanut-like structure. From Fig. 2d, we can see that, a small layer of nanoparticles, namely NiWO_4 nanoparticles, is newly loaded on the surface of composite $g\text{-C}_3\text{N}_4/\text{TiO}_2$ to form a ternary heterojunction composite $g\text{-C}_3\text{N}_4/\text{TiO}_2/\text{NiWO}_4$. Meanwhile, EDS spectrum of the as-prepared $g\text{-C}_3\text{N}_4/\text{TiO}_2/\text{NiWO}_4$ show the existence of C, N, O, W, Ti, and Ni in the composite, indicating that the uniform dispersion of these five elements (Fig. 3). These results together with XRD analysis can demonstrate that the ternary heterojunction photocatalyst was successfully prepared.

3.2 FT-IR spectra

FT-IR spectra of the samples $g\text{-C}_3\text{N}_4$, $g\text{-C}_3\text{N}_4/\text{TiO}_2$ and $g\text{-C}_3\text{N}_4/\text{TiO}_2/\text{NiWO}_4$ are shown in Fig. 4.

From Fig. 4, we can see that, the peak at around 3430 cm^{-1} is related to hydroxyl groups, which can be attributed to the tensile vibration of adsorbed water molecules [27, 28]. The broad absorption peaks between 2900 and 3300 cm^{-1} correspond to the $-\text{NH}_2$ and $=\text{NH}$ stretching vibrations [29]. It can also easily be seen from Fig. 4, $g\text{-C}_3\text{N}_4$ contains a small amount

Fig. 2 SEM images of g-C₃N₄ (a), g-C₃N₄/TiO₂ (b, c) and g-C₃N₄/TiO₂/NiWO₄ (d)

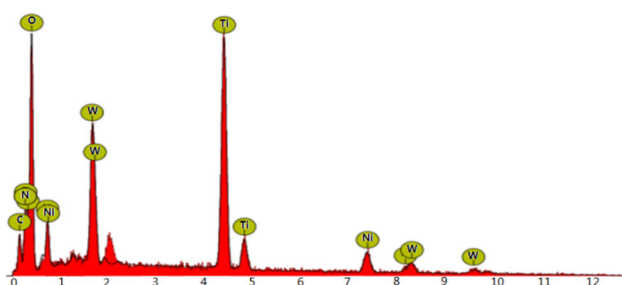
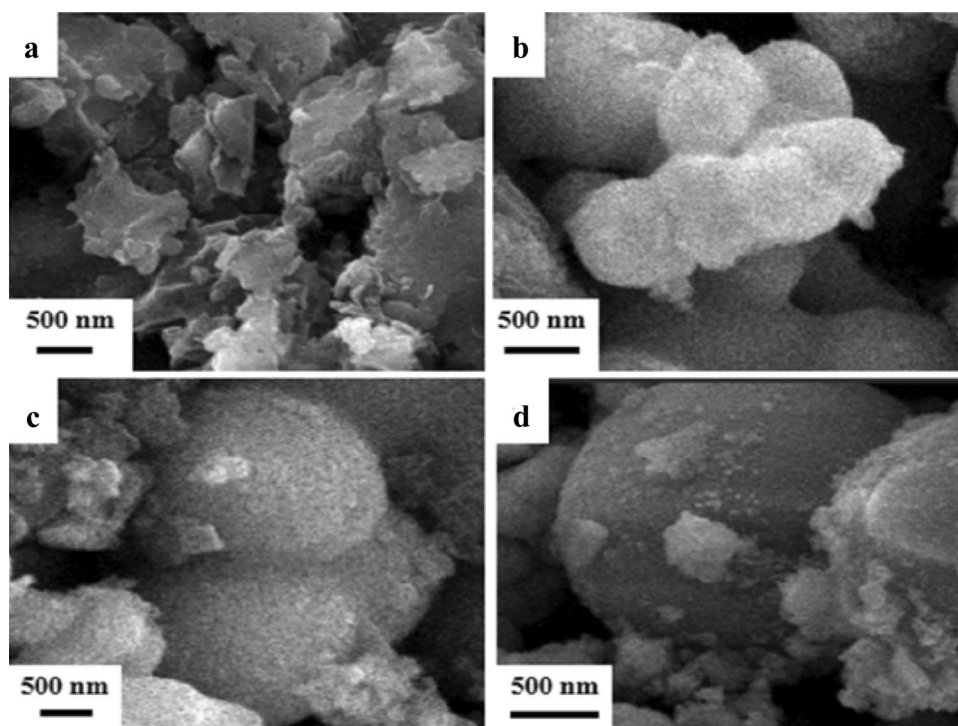


Fig. 3 EDS image of composite g-C₃N₄/TiO₂/NiWO₄

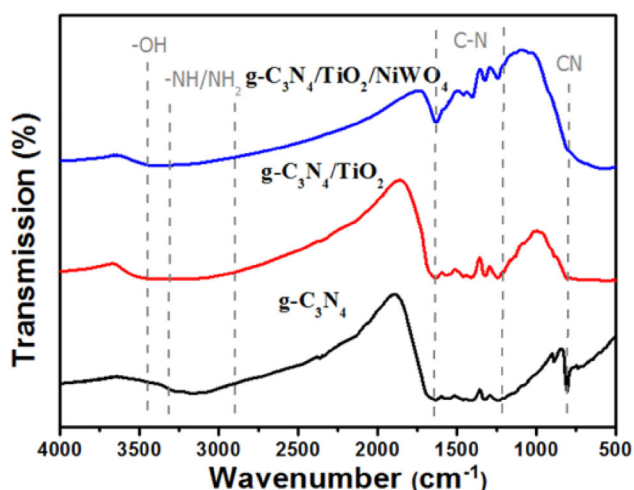


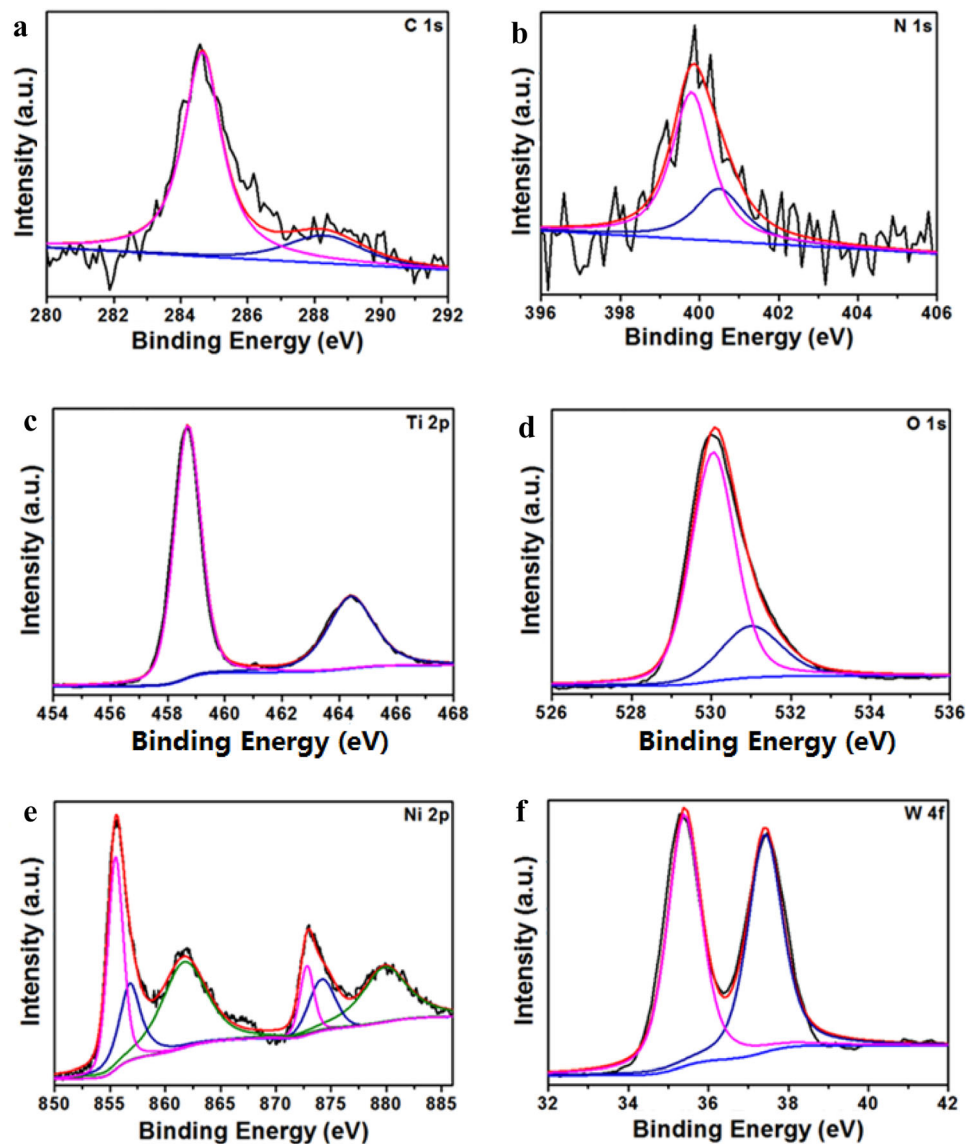
Fig. 4 FT-IR spectra of g-C₃N₄, g-C₃N₄/TiO₂ and g-C₃N₄/TiO₂/NiWO₄

of amino groups, while amino groups cannot be seen from the FT-IR spectra of composites g-C₃N₄/TiO₂ and g-C₃N₄/TiO₂/NiWO₄. This is mainly related to the low content of g-C₃N₄ in composite g-C₃N₄/TiO₂ and g-C₃N₄/TiO₂/NiWO₄. The absorption peak in the range of 1200 cm⁻¹ to 1650 cm⁻¹ is caused by the stretching vibration of the C–N heterocycle [30]. After being combined with TiO₂, the characteristic peak of C–N heterocycle in composite g-C₃N₄/TiO₂ is still obvious. After being combined with NiWO₄, the strength of C–N heterocycle in composite g-C₃N₄/TiO₂/NiWO₄ is weakened, but still obvious, indicating that the C–N heterocycle in the composite is relatively stable. The peak at 807 cm⁻¹ can correspond to the stretching vibration of the triazine ring [31]; it is worth noting that the triazine ring characteristic peaks cannot be observed in FT-IR spectra of the composites g-C₃N₄/TiO₂ and g-C₃N₄/TiO₂/NiWO₄, indicating that the triazine ring structure in g-C₃N₄ is destroyed during the combined process with TiO₂.

3.3 XPS analysis

X-ray photoelectron spectroscopy (XPS) technique was employed to investigate the surface chemical compositions and valence state of g-C₃N₄/TiO₂/NiWO₄. The C 1s spectra (Fig. 5a) showed 2 peaks.

Fig. 5 XPS spectra of C, N, Ti, O, Ni, and W elements in g-C₃N₄/TiO₂/NiWO₄ sample



The peak at 284.8 eV can be assigned to C=C bond or indefinite-form carbon, which originate from instrument itself. The peaks at 288.4 eV can be ascribed to the N-C=N bond [32].

From Fig. 5b, we can see that, the N 1s region can be divided into two different peaks at 399.6 and 400.8 eV, which correspond to N-(C)₃ and C-N-H groups, respectively [33].

In the Ti 2p spectra shown in Fig. 5c, the two peaks of 2p_{3/2} and 2p_{1/2} at binding energies of 458.4 and 464.3 eV, respectively, can be attributed to Ti⁴⁺ in the composite [34].

As shown in Fig. 5d, the dominant peak of O 1s locates at binding energy of 529.6 eV, which suggests the lattice oxygen O²⁻. The other peak at

531.6 eV is assigned hydroxyl groups absorbed in the surface.

There are six peaks at binding energies of 880.5, 873.5, 869.7, 861.8, 855.6, and 853.0 eV for Ni 2p element (Fig. 5e), respectively. The two peaks located at 855.6 and 873.5 eV, respectively, indicate that there exist Ni ions in bivalent status.

From Fig. 5f we can see that, the W 4f spectra were fitted by two peaks centered around 34.9 eV and 37.1 eV, which can be ascribed to W 4f_{7/2} and W 4f_{5/2}, respectively, representing the presence of W⁶⁺, that formed NiWO₄ together with Ni²⁺ and O²⁻ [35].

Based on the above-mentioned XPS results, it is reasonable to assert that the sample is indeed a

ternary heterojunction composite photocatalyst $g\text{-C}_3\text{N}_4/\text{TiO}_2/\text{NiWO}_4$.

3.4 UV–Vis spectra analysis

The optical absorption properties of $g\text{-C}_3\text{N}_4$, TiO_2 , NiWO_4 , $g\text{-C}_3\text{N}_4/\text{TiO}_2$, and $g\text{-C}_3\text{N}_4/\text{TiO}_2/\text{NiWO}_4$ was studied by UV–Vis spectra and displayed in Fig. 6a. The absorption band edges of $g\text{-C}_3\text{N}_4$, TiO_2 , and NiWO_4 are located at around 445 nm, 378 nm, and 430 nm, respectively. However, $g\text{-C}_3\text{N}_4/\text{TiO}_2/\text{NiWO}_4$ exhibits a red shift toward longer wavelength compared with $g\text{-C}_3\text{N}_4$ and TiO_2 , indicating that the introduction of NiWO_4 can promote the light absorption of the photocatalyst under visible light.

The Tauc's bandgap plots of the samples $g\text{-C}_3\text{N}_4$, TiO_2 , and NiWO_4 is converted from the UV–Vis diffuse reflectance absorption spectra (DRS) according to the Kubelka–Munk function. As shown in Fig. 6b–d, the bandgap energy of $g\text{-C}_3\text{N}_4$, TiO_2 , and NiWO_4 is estimated to be 2.78 eV, 3.29 eV, and 2.89 eV respectively.

3.5 Photocatalytic degradation of RhB and reusability of as-prepared catalyst

RhB in aqueous solutions were selected as the target pollutant to evaluate the photocatalytic performance of the as-prepared catalysts under visible-light irradiation.

From Fig. 7a we can see that, after visible-light irradiation for 60 min, 12%, 72%, and 41% of RhB are degraded by using pure NiWO_4 , $g\text{-C}_3\text{N}_4$, and P25 TiO_2 as photocatalyst, respectively. Both binary and ternary photocatalysts exhibit enhanced photocatalytic activity, and the degradation efficiencies of RhB can all reach 99% after visible-light irradiation for 40 min. But, obviously, the degradation rate of ternary photocatalyst $g\text{-C}_3\text{N}_4/\text{TiO}_2/\text{NiWO}_4$ is faster than that of binary photocatalyst $g\text{-C}_3\text{N}_4/\text{TiO}_2$.

The stability of the ternary composite photocatalyst was a significant factor for its practical application. In order to assess the photocatalytic stability of $g\text{-C}_3\text{N}_4/\text{TiO}_2/\text{NiWO}_4$, a cycling experiment for photocatalytic degradation of RhB was carried out.

As shown in Fig. 7b, after five cycles, the composite photocatalyst $g\text{-C}_3\text{N}_4/\text{TiO}_2/\text{NiWO}_4$ shows a little or even no deactivation, indicating that the composite photocatalyst $g\text{-C}_3\text{N}_4/\text{TiO}_2/\text{NiWO}_4$ is stable during

Fig. 6 UV–Vis spectra (a) of the samples and the bandgaps of $g\text{-C}_3\text{N}_4$ (b), TiO_2 (c) and NiWO_4 (d) estimated using the Tauc plot

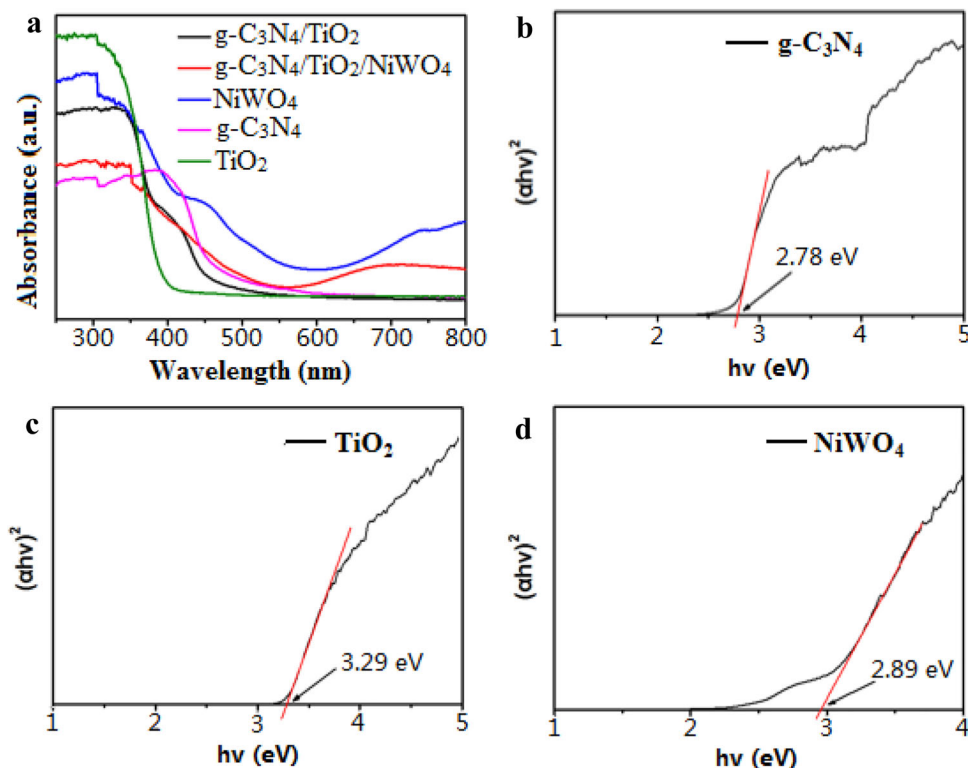
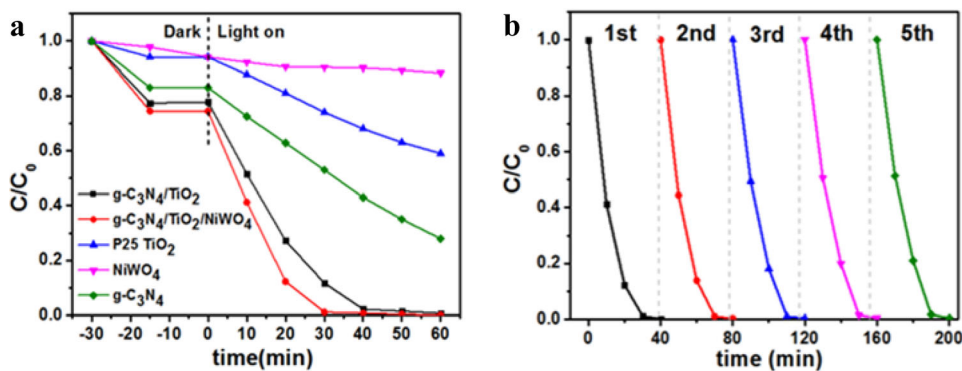


Fig. 7 **a** Photocatalytic performances toward the photodegradation of RhB with different catalyst under visual light irradiation and **b** the cycling experiment for RhB degradation using $g\text{-C}_3\text{N}_4/\text{TiO}_2/\text{NiWO}_4$ as a photocatalyst



the photocatalytic reaction. Therefore, the as-prepared ternary heterojunction composite $g\text{-C}_3\text{N}_4/\text{TiO}_2/\text{NiWO}_4$ could be employed as an efficient photocatalyst for application in organic pollutant removal.

3.6 Photoluminescence spectra analysis

In order to further investigate the reasons for the improvement of photocatalytic performance of the as-prepared $g\text{-C}_3\text{N}_4/\text{TiO}_2/\text{NiWO}_4$, the fluorescence spectra of $g\text{-C}_3\text{N}_4$, $g\text{-C}_3\text{N}_4/\text{TiO}_2$ and $g\text{-C}_3\text{N}_4/\text{TiO}_2/\text{NiWO}_4$ were analyzed.

As seen in Fig. 8, for pure $g\text{-C}_3\text{N}_4$, fluorescence intensity was relatively higher, indicating a lower separation rate of photogenerated carriers. The composite $g\text{-C}_3\text{N}_4/\text{TiO}_2$ exhibited lower PL intensity; $g\text{-C}_3\text{N}_4/\text{TiO}_2/\text{NiWO}_4$ displayed the lowest fluorescence signal, suggesting that the construction of the ternary heterojunction photocatalyst can effectively

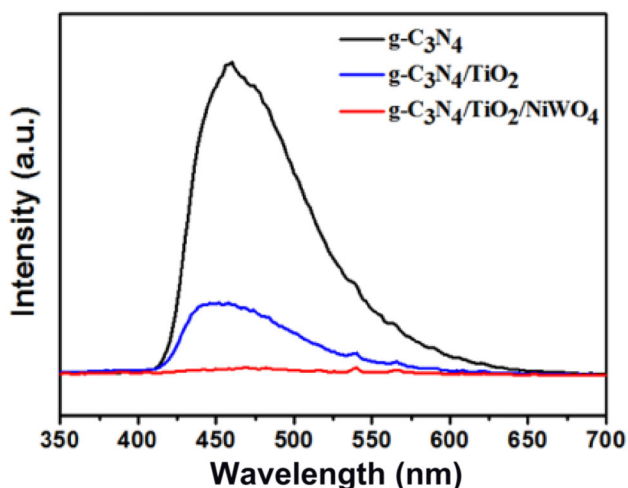


Fig. 8 Photoluminescence spectra of $g\text{-C}_3\text{N}_4$, $g\text{-C}_3\text{N}_4/\text{TiO}_2$ and $g\text{-C}_3\text{N}_4/\text{TiO}_2/\text{NiWO}_4$

suppress the recombination of the photogenerated electron–hole pairs and improve the photocatalytic activity of the catalyst [36].

3.7 Photocurrent and electrochemical impedance measurements

The surface charge separation and transfer efficiencies of the as-prepared materials were further investigated by transient photocurrent responses and electrochemical impedance spectroscopy. As shown in Fig. 9a, $g\text{-C}_3\text{N}_4/\text{TiO}_2/\text{NiWO}_4$ possesses the highest photocurrent intensity. The semicircular radius in the impedance spectra of $g\text{-C}_3\text{N}_4/\text{TiO}_2/\text{NiWO}_4$ was obviously smaller than that of binary photocatalyst, suggesting an efficient interfacial charge transport resistance (Fig. 9b) [37–39].

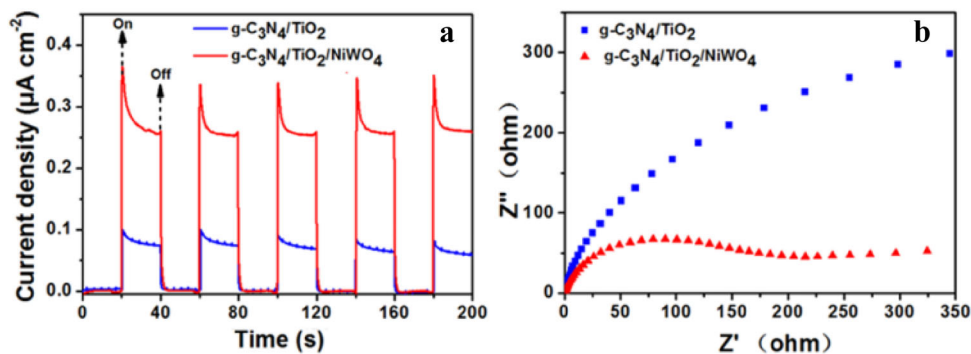
The above-mentioned results demonstrate that the construction of the ternary heterojunction photocatalyst can accelerate the interfacial transfer and separation of charge carriers in hybrid photocatalyst.

3.8 Active species trapping experiments and photocatalytic mechanism for the as-prepared composite

At present research, radical species trapping experiments were carried out to study the photocatalytic mechanism of the composite $g\text{-C}_3\text{N}_4/\text{TiO}_2/\text{NiWO}_4$ for the degradation of RhB solution. In the trapping experiments, isopropyl alcohol (IPA), ethylenediaminetetraacetic acid disodium (EDTA-2Na), and ascorbic acid (VC) were separately used as scavenger of $\cdot\text{OH}$, h^+ , and $\cdot\text{O}_2^-$, respectively.

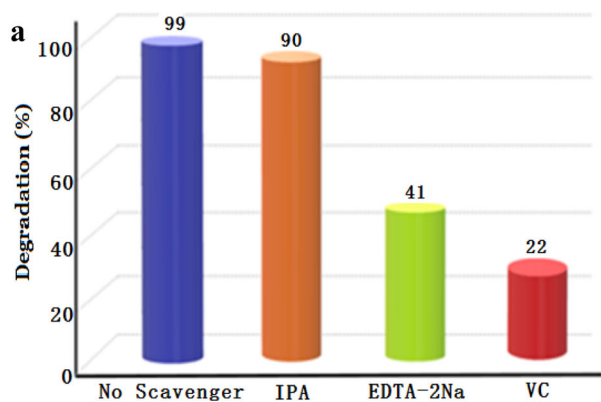
As shown in Fig. 10a, 99% of RhB in solutions can be removed by the $g\text{-C}_3\text{N}_4/\text{TiO}_2/\text{NiWO}_4$ without scavengers during 30 min. When IPA is added into the RhB solutions, there was no dramatic decrease in

Fig. 9 **a** Transient photocurrent responses and **b** EIS changes of g-C₃N₄, TiO₂, NiWO₄, g-C₃N₄/TiO₂, and g-C₃N₄/TiO₂/NiWO₄ samples



the photocatalytic activity, the degradation efficiency of RhB decreased from 99 to 90% during 30 min, implying that ·OH contributes just a little during photocatalysis. While the introduction of EDTA-2Na

and VC to RhB solutions made the degradation efficiencies dropped from 99 to 41% and 22%, respectively, indicating that the h⁺ and ·O₂⁻ play an important role in RhB degradation process.



Based on the above analysis, a possible mechanism for the degradation of RhB is proposed as illustrated in Fig. 10b. Under visible-light irradiation, both g-C₃N₄ and NiWO₄ in the composite photocatalyst g-C₃N₄/TiO₂/NiWO₄ absorb photons of energy greater than the corresponding bandgap energy, which excite the electrons in the VB to the CB and then leave holes in the VB. The bandgap of TiO₂ is too wide to be excited by visible light to produce photogenerated electron–hole pairs. The conduction band position of TiO₂ (−0.51 eV) is more positive than that of g-C₃N₄ (−1.15 eV) and NiWO₄ (−1.05 eV), so the photoexcited electrons (e⁻) will transfer from the CB of g-C₃N₄ and NiWO₄ to the CB of TiO₂. Thereby, the recombination of photogenerated electron–hole pairs in g-C₃N₄ and NiWO₄ can be effectively suppressed. The dissolved oxygen (O₂) in RhB solutions can be trapped by electrons (e⁻) accumulated in the CB of TiO₂ and generated ·O₂⁻ to degrade RhB, while the holes (h⁺) remaining on the VB of g-C₃N₄ and NiWO₄ can directly oxidize RhB. The degradation process of RhB is as follows:

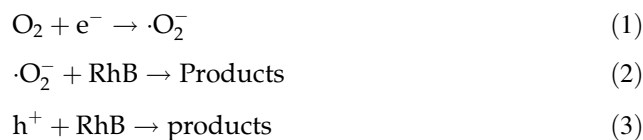
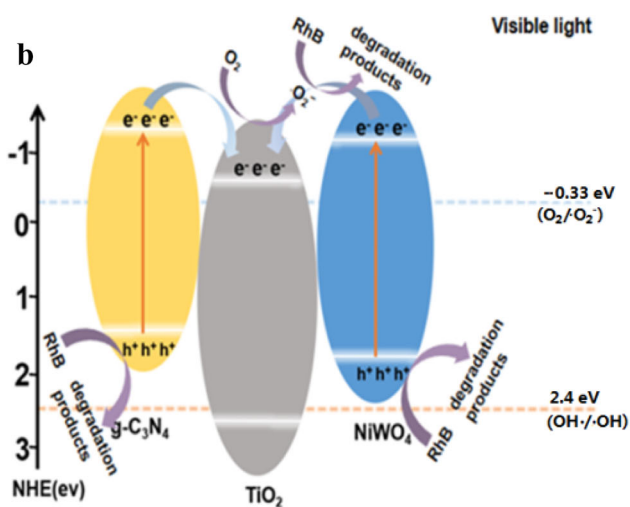


Fig. 10 **a** Trapping experiment of active species during the photocatalytic degradation of RhB with g-C₃N₄/TiO₂/NiWO₄. **b** Photocatalytic mechanism for g-C₃N₄/TiO₂/NiWO₄ composite photocatalyst

4 Conclusions

In conclusion, a novel photocatalyst g-C₃N₄/TiO₂/NiWO₄ could be successfully fabricated by using a simple hydrothermal method. By constructing the

ternary heterojunction composite photocatalyst, the electron migration rate and light absorption of the composite material are further improved; the photo-generated electron–hole recombination is inhibited. The resulting g-C₃N₄/TiO₂/NiWO₄ exhibit enhanced photocatalytic activity for the degradation of RhB under visible light compared with the photocatalyst g-C₃N₄, TiO₂, NiWO₄, and g-C₃N₄/TiO₂. Moreover, the as-prepared composite shows a very strong stability and reusability. In addition, we concluded that the h⁺ and ·O₂⁻ radicals are the main active species of the composite g-C₃N₄/TiO₂/NiWO₄ in aqueous solution under visible-light irradiation by trapping experiments for radicals and holes. Our work provides a new perception on designing ternary heterojunction composite photocatalyst with superior photocatalytic performance to deal with the environmental pollution issues.

Acknowledgements

This work was supported by Postgraduate Research & Practice Innovation Program of Jiangsu Province (KYCX18_2340).

Author contributions

All authors contributed to the study conception and design. Material preparation, data collection and analysis were performed by H-CG, Y-BT and F-YC. The first draft of the manuscript was written by H-CG and all authors commented on previous versions of the manuscript. All authors read and approved the final manuscript.

Data availability

The data used to support the findings of this study are available from the corresponding author upon request.

Declarations

Conflict of interest There are no conflicts of interest to declare.

References

1. A. Ojha, M. Thakker, D.O. Shah, P. Thareja, Flow-directed assembly of non-spherical titania nanoparticles into super-hydrophilic thin films, *Front. Mater. Sci.* **10**, 1–7 (2016)
2. Z.P. Tshabalala, K. Shingange, B.P. Dhonge, O.M. Ntwaeaborwa, G.H. Mhlongo, D.E. Motaung, Fabrication of ultra-high sensitive and selective CH₄ room temperature gas sensing of TiO₂ nanorods: detailed study on the annealing temperature. *Sens. Actuators B* **238**, 402–419 (2017)
3. J.M. Meichtry, N. Quici, G. Mailhot, M.I. Litter, Heterogeneous photocatalytic degradation of citric acid over TiO₂. I: mechanism of 3-oxoglutaric acid degradation. *Appl. Catal. B* **102**, 454–463 (2011)
4. W.T. Sun, Y. Yu, H.Y. Pan, X.F. Gao, Q. Chen, L.M. Peng, CdS quantum dots sensitized TiO₂ nanotube-array photoelectrodes. *J. Am. Chem. Soc.* **130**, 1124–1125 (2008)
5. G.L. Chen, W.T. Zhong, Y.S. Li, Q. Deng, X. Ou, Q.C. Pan, X.W. Wang, X.H. Xiong, C.H. Yang, M.L. Liu, Rational design of TiO–TiO₂ heterostructure/polypyrrole as a multifunctional sulfur host for advanced lithium–sulfur batteries. *ACS Appl. Mater. Interface* **11**, 5055–5063 (2019)
6. L. Zhang, D.W. Jing, X.L. She, H.W. Liu, D.J. Yang, Y. Lu, J. Li, Z.F. Zheng, L.J. Guo, Heterojunctions in g-C₃N₄/TiO₂ (B) nanofibres with exposed (001) plane and enhanced visible-light photoactivity. *J. Mater. Chem. A* **2**, 2071–2078 (2014)
7. R. Plugaru, A. Cremades, J. Piqueras, The effect of annealing in different atmospheres on the luminescence of polycrystalline TiO₂. *J. Phys. Condens. Mater.* **16**, S261–S268 (2004)
8. H.Q. Xu, J.H. Hu, D.K. Wang, Z.H. Li, Q. Zhang, Y. Luo, S.H. Yu, H.L. Jiang, Visible-light photoreduction of CO₂ in a metal-organic framework: boosting electron–hole separation via electron trap states. *J. Am. Chem. Soc.* **137**, 13440–13443 (2015)
9. Y. Zheng, J. Liu, J. Liang, M. Jaroniec, Graphitic carbon nitride materials: controllable synthesis and applications in fuel cells and photocatalysis. *Energy Environ. Sci.* **5**, 6717–6731 (2012)
10. H.J. Wang, X. Li, X.X. Zhao, C.Y. Li, X.H. Song, P. Zhang, P.W. Huo, X. Li, A review on heterogeneous photocatalysis for environmental remediation: from semiconductors to modification strategies. *Chin. J. Catal.* **43**, 178–214 (2022)
11. Z. Zhu, Z.X. Liu, X. Tang, K. Reeti, P.W. Huo, J.W.C. Wong, J. Zhao, Sulfur-doped g-C₃N₄ for efficient photocatalytic CO₂ reduction: insights by experiment and first-principles calculations. *Catal. Sci. Technol.* **11**, 1725–1736 (2021)
12. J.Y. Lei, B. Chen, W.J. Lv, L. Zhou, L.Z. Wang, Y.D. Liu, J.L. Zhang, An inverse opal TiO₂/g-C₃N₄ composite with a

- heterojunction for enhanced visible light-driven photocatalytic activity. *Dalton Trans.* **48**, 3486–3495 (2019)
13. Q. Zhang, H. Wang, S. Chen, Y. Su, X. Quan, Three-dimensional TiO₂ nanotube arrays combined with g-C₃N₄ quantum dots for visible light-driven photocatalytic hydrogen production. *RSC Adv.* **7**, 13223–13227 (2017)
 14. T. Wang, T.Y. Sun, J.H. Xu, H. Xiao, Z.M. Zhang, H.Q. Bian, H.H. Ding, The pre-acidizing corrosion on the surface of TiO₂ enhanced the photocatalytic activity of g-C₃N₄/TiO₂. *J. Mater. Sci.* **32**, 21083–21092 (2021)
 15. Y.G. Tan, Z. Shu, J. Zhou, T.T. Li, W.B. Wang, Z.L. Zhao, One-step synthesis of nanostructured g-C₃N₄/TiO₂ composite for highly enhanced visible-light photocatalytic H₂ evolution. *Appl. Catal. B* **230**, 260–268 (2018)
 16. W.P. Zhang, X.Y. Xiao, Y. Li, X.Y. Zeng, L.L. Zheng, C.X. Wan, Liquid-exfoliation of layered MoS₂ for enhancing photocatalytic activity of TiO₂/g-C₃N₄ photocatalyst and DFT study. *Appl. Surf. Sci.* **389**, 496–506 (2016)
 17. M. Mohamed Jaffer Sadiq, U. Sandhya Shenoy, D. Krishna Bhat, Novel RGO-ZnWO₄-Fe₃O₄ nanocomposite as high performance visible light photocatalyst. *RSC Adv.* **6**, 61821–61829 (2016)
 18. D.Y. Wu, J.Z. Li, J.R. Guan, C.Y. Liu, X.X. Zhao, Z. Zhu, C.C. Ma, P.W. Huo, C.X. Li, Y.S. Yan, Improved photoelectric performance via fabricated heterojunction g-C₃N₄/TiO₂/HNTs loaded photocatalysts for photodegradation of ciprofloxacin. *J. Ind. Eng. Chem.* **64**, 206–218 (2018)
 19. A.A. Kaminskii, H.J. Eichler, K.I. Ueda, N.V. Klassen, B.S. Redkin, L.E. Li, J. Findeisen, D. Jaque, J. García-Sole, J. Fernández, R. Balda, Properties of Nd³⁺-doped and undoped tetragonal PbWO₄, NaY(WO₄)₂, CaWO₄, and undoped monoclinic ZnWO₄ and CdWO₄ as laser-active and stimulated raman scattering-active crystals. *Appl. Opt.* **38**, 4533–4547 (1999)
 20. M. Hao, X. Meng, Y. Miao, Synthesis of NiWO₄ powder crystals of polyhedron for photocatalytic degradation of rhodamine. *Solid State Sci.* **72**, 103–108 (2017)
 21. M. Eghbali-Arani, A. Sobhani-Nasab, M. Rahimi-Nasrabadi, F. Ahmadi, S. Pourmasoud, Ultrasound-assisted synthesis of YbVO₄ nanostructure and YbVO₄/CuWO₄ nanocomposites for enhanced photocatalytic degradation of organic dyes under visible light. *Ultrason. Sonochem.* **43**, 120–135 (2018)
 22. J. Wan, X. Du, R.M. Wang, E.Z. Liu, J. Jia, X. Bai, X.Y. Hu, J. Fan, Mesoporous nanoplate multi-directional assembled Bi₂WO₆ for high efficient photocatalytic oxidation of NO. *Chemosphere* **193**, 737–744 (2018)
 23. M.M. Mohamed, S.A. Ahmed, K.S. Khairou, Unprecedented high photocatalytic activity of nanocrystalline WO₃/NiWO₄ hetero-junction towards dye degradation: effect of template and synthesis conditions. *Appl. Catal. B* **150–151**, 63–73 (2014)
 24. Y.J. Cui, G.G. Zhang, Z.Z. Lin, X.C. Wang, Condensed and low-defected graphitic carbon nitride with enhanced photocatalytic hydrogen evolution under visible light irradiation. *Appl. Catal. B* **181**, 413–419 (2015)
 25. C.Q. Li, Z.M. Sun, W.Z. Zhang, C.H. Yu, S.L. Zheng, Highly efficient g-C₃N₄/TiO₂/kaolinite composite with novel three-dimensional structure and enhanced visible light responding ability towards ciprofloxacin and *S. aureus*. *Appl. Catal. B* **220**, 272–282 (2018)
 26. M.I. Ahmed, A. Adam, A. Khan, M.N. Siddiqui, Z.H. Yamani, M. Qamar, Synthesis of mesoporous NiWO₄ nanocrystals for enhanced photoelectrochemical water oxidation. *Mater. Lett.* **177**, 135–138 (2016)
 27. Y.P. Zhang, C.X. Pan, TiO₂/graphene composite from thermal reaction of graphene oxide and its photocatalytic activity in visible light. *J. Mater. Sci.* **46**, 2622–2626 (2010)
 28. D.J. Cooke, D. Eder, J.A. Elliott, Role of benzyl alcohol in controlling the growth of TiO₂ on carbon nanotubes. *J. Phys. Chem. C* **114**, 2462–2470 (2010)
 29. Q.H. Liang, Z. Li, Y. Bai, Z.H. Huang, F.Y. Kang, Q.H. Yang, A composite polymeric carbon nitride with in situ formed isotype heterojunctions for highly improved photocatalysis under visible light. *Small* **13**, 1603182 (2017)
 30. Y. Wang, X. Wang, M. Antonietti, Polymeric graphitic carbon nitride as a heterogeneous organocatalyst: from photochemistry to multipurpose catalysis to sustainable chemistry. *Angew Chem. Int. Ed. Engl.* **51**, 68–89 (2012)
 31. X.F. Chen, J.S. Zhang, X.Z. Fu, M. Antonietti, X.C. Wang, Fe-g-C₃N₄-catalyzed oxidation of benzene to phenol using hydrogen peroxide and visible light. *J. Am. Chem. Soc.* **131**, 11658–11659 (2009)
 32. F. Dong, L.W. Wu, Y.J. Sun, M. Fu, Z.B. Wu, S.C. Lee, Efficient synthesis of polymeric g-C₃N₄ layered materials as novel efficient visible light driven photocatalysts. *J. Mater. Chem.* **21**, 15171–15174 (2011)
 33. H.H. Ji, F. Chang, X.F. Hu, W. Qin, J.W. Shen, Photocatalytic degradation of 2,4,6-trichlorophenol over g-C₃N₄ under visible light irradiation. *Chem. Eng. J.* **218**, 183–190 (2013)
 34. R.R. Hao, G.H. Wang, H. Tang, L.L. Sun, C. Xu, D.Y. Han, Template-free preparation of macro/mesoporous g-C₃N₄/TiO₂ heterojunction photocatalysts with enhanced visible light photocatalytic activity. *Appl. Catal. B* **187**, 47–58 (2016)
 35. X.S. Feng, Y. Huang, M.H. Chen, X.F. Chen, C. Li, S.H. Zhou, X.G. Gao, Self-assembly of 3D hierarchical MnMoO₄/NiWO₄ microspheres for high-performance supercapacitor. *J. Alloy Compd.* **763**, 801–807 (2018)
 36. Y. Liu, Z.H. Yang, P.P. Song, R. Xu, H. Wang, Facile synthesis of Bi₂MoO₆/ZnSnO₃ heterojunction with enhanced

- visible light photocatalytic degradation of methylene blue. *Appl. Surf. Sci.* **430**, 561–570 (2018)
37. M.Y. Li, Y.B. Tang, W.L. Shi, F.Y. Chen, Y. Shi, H.C. Gu, Design of visible-light-response core–shell $\text{Fe}_2\text{O}_3/\text{CuBi}_2\text{O}_4$ heterojunctions with enhanced photocatalytic activity towards the degradation of tetracycline: Z-scheme photocatalytic mechanism insight. *Inorg. Chem. Front.* **5**, 3148–3154 (2018)
38. J. Xu, B.F. Luo, W. Gu, Y.P. Jian, F.L. Wu, Y.B. Tang, H. Shen, Fabrication of $\text{In}_2\text{S}_3/\text{NaTaO}_3$ composites for enhancing the photocatalytic activity toward the degradation of tetracycline. *New. J. Chem.* **42**, 5052–5058 (2018)
39. F.Y. Chen, X. Zhang, Y.B. Tang, X.G. Wang, K.K. Shu, Facile and rapid synthesis of a novel spindle-like heterojunction BiVO_4 showing enhanced visible-light-driven photoactivity. *RSC Adv.* **10**, 5234–5240 (2020)

Publisher's Note Springer Nature remains neutral with regard to jurisdictional claims in published maps and institutional affiliations.